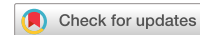


communications

earth & environment

ARTICLE



<https://doi.org/10.1038/s43247-021-00232-5>

OPEN

Mediterranean heat injection to the North Atlantic delayed the intensification of Northern Hemisphere glaciations

Stefanie Kaboth-Bahr^{1,8✉}, André Bahr^{2,8}, Christian Stepanek³, Maria Carolina Amorim Catunda², Cyrus Karas⁴, Martin Ziegler⁵, Ángela García-Gallardo⁶ & Patrick Grunert⁷

The intensification of Northern Hemisphere glaciations at the end of the Pliocene epoch marks one of the most substantial climatic shifts of the Cenozoic. Despite global cooling, sea surface temperatures in the high latitude North Atlantic Ocean rose between 2.9–2.7 million years ago. Here we present sedimentary geochemical proxy data from the Gulf of Cadiz to reconstruct the variability of Mediterranean Outflow Water, an important heat source to the North Atlantic. We find evidence for enhanced production of Mediterranean Outflow from the mid-Pliocene to the late Pliocene which we infer could have driven a sub-surface heat channel into the high-latitude North Atlantic. We then use Earth System Models to constrain the impact of enhanced Mediterranean Outflow production on the northward heat transport in the North Atlantic. In accord with the proxy data, the numerical model results support the formation of a sub-surface channel that pumped heat from the subtropics into the high latitude North Atlantic. We further suggest that this mechanism could have delayed ice sheet growth at the end of the Pliocene.

¹ Institute of Geosciences, University of Potsdam, Potsdam-Golm, Germany. ² Institute of Earth Sciences, Heidelberg University, Heidelberg, Germany. ³ Alfred Wegener Institute, Helmholtz Centre for Polar and Marine Research, Bremerhaven, Germany. ⁴ Universidad de Santiago de Chile, Santiago, Chile. ⁵ Department of Earth Sciences, Utrecht University, Utrecht, The Netherlands. ⁶ Instituto de Ciencias del Mar y Limnología, Universidad Nacional Autónoma de México, Mexico City, Mexico. ⁷ Institute of Geology and Mineralogy, University of Cologne, Cologne, Germany. [✉]These authors contributed equally: Stefanie Kaboth-Bahr, André Bahr. [✉]email: kabothbahr@uni-potsdam.de

The intensified growth of Northern Hemisphere ice sheets (iNHG; ~3.2–2.4 Ma (million years ago)) towards the end of the Pliocene marks the onset of the profound glacial–interglacial fluctuations that are characteristic for the subsequent Pleistocene epoch¹. The acceleration of Northern Hemisphere ice sheet growth is proposed to have been triggered by a simultaneous global atmospheric cooling trend linked to, firstly, a steady decline in atmospheric carbon dioxide concentration starting at ~4.0 Ma ($p\text{CO}_2$; see Fig. 1)^{2–4}. Secondly, it has been proposed that the strength of the global oceanic conveyor belt weakened starting at ~4–3 Ma, which lowered the heat and moisture exchange between ocean and atmosphere^{5,7}. Despite the proposed decline of the oceanic heat transport and $p\text{CO}_2$ during the Plio–Pleistocene transition, which provides ideal background conditions to support the iNHG, the high-latitude North Atlantic (>50°N) experienced a strong sea surface warming (2–3 °C relative to present day) between ~2.9 and 2.7 Ma (cf. ODP Site 982 in Fig. 1; for other high-latitude SST records see Fig. S1)⁸. This anomalous sea surface temperature (SST) increase most likely led to higher Arctic and sub-Arctic air temperatures, which in turn could have delayed the formation of major ice sheets in the Northern Hemisphere^{5,9}. In fact, the intensification of ice sheet development on Greenland, Scandinavia and North America only accelerated after ~2.7 Ma during glacials G6–G4 subsequent to the North Atlantic SST warming event (Fig. 1)^{10,11}.

The anomalous surface warming of the high-latitude North Atlantic contrasts the relatively steady decline in $p\text{CO}_2$ between ~3.2 and 2.4 Ma, and thus argues against $p\text{CO}_2$ as a dominant driver of high-latitude SST variability (Fig. 1). The SST increase at

high latitudes in the North Atlantic could also result from a transitory invigoration of the Atlantic Meridional Overturning Circulation (AMOC) as its strength modulates the northward directed heat transport¹². AMOC-driven SST anomalies are expected to lead to synchronous SST changes in mid- (~40°N) and high-latitude (~60°N) regions of the North Atlantic¹³. However, the mid-latitude North Atlantic did not experience a similar amplitude surface warming as the high latitudes (cf. IODP Site U1313 in Fig. 1; for other mid-latitude SST records see Fig. S1) between ~2.9 and 2.7 Ma, arguing against a strong oceanic overturning circulation being responsible for the entire magnitude of the reconstructed high-latitude SST warming. Similarly, a potential northward shift of the arctic front, facilitating protrusion of warm subtropical waters into the high latitudes, is at odds with the inferred southward shift of the North Atlantic frontal systems during the Late Pliocene glacials¹⁴. Alternatively, the high-latitude SST warming between ~2.9 and 2.7 Ma could potentially be related to the closure of the Central American Seaway (CAS) and Arctic gateways (e.g. Bering Strait and Canadian Archipelago), which have been argued to facilitate high-latitude warming in the North Atlantic via an intensified Gulfstream/North Atlantic Current^{15,16}. However, the anomalous SST warming between ~2.9 and 2.7 Ma does not coincide with a presumed closure of the Arctic gateways during the M2 event (~3.3 Ma)¹⁷ and clearly postdates the main phase of constriction of the CAS that occurred from 4.8 to 3.8 Ma⁵. In fact, during the Late Pliocene, and our studied time frame, the CAS sill depth fell most likely below 100 m⁵ prior to its final closure, and thus did no longer have a substantial pull on AMOC strength as it presumably did during the Early Pliocene^{18,19}. Hence, the observed

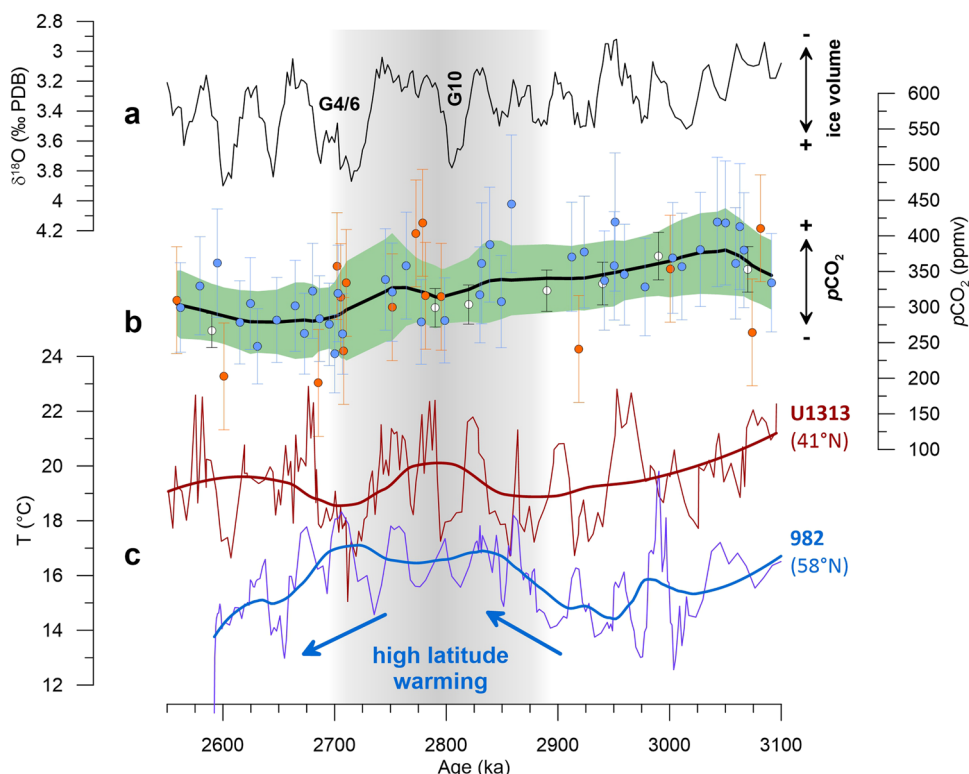


Fig. 1 Overview of global climate dynamics during the Plio-Pleistocene transition. a Ice volume reconstruction with Glacials G4/6 and G10 denoted⁴⁴. **(b)** different atmospheric $p\text{CO}_2$ reconstructions for the Plio-Pleistocene transition (white circles;² orange circles;³ blue circles⁴); with LOESS smoother (black line; smoothing factor 0.07) and 95% confidence interval (green shading) derived from a Monte Carlo Simulation with 1000 iterations. **c** Sea surface temperature (SST) records of mid-latitude Site U1313 (dark red line; thick line indicates 0.5 LOESS smoother; see Fig. 2 for site location)⁴³ and high-latitude Site ODP 982 (blue line; thick line indicates 0.3 LOESS smoother; see Fig. 2 for site location)⁶⁴ on the revised age model of⁴¹. The grey shading indicates the interval of anomalous SST warming in the high-latitude North Atlantic as depicted by blue arrows.

delay in Northern Hemisphere ice sheet growth against the backdrop of global cooling and reduced northward heat transport requires an additional but yet unknown process that specifically alters surface-water temperatures in the high-latitude North Atlantic.

A possible candidate to explain the SST warming of the high-latitude North Atlantic between ~2.9 and 2.7 Ma could be the intrusion of dense and warm Mediterranean Outflow Water (MOW) into the central North Atlantic. MOW originates from warm and saline intermediate- to deep-water masses of the eastern and western Mediterranean Sea and enters the North Atlantic via the Strait of Gibraltar²⁰ at water depths of ~800–1200 m (Fig. 2)²¹. Modern observational data show that the injection of Mediterranean-sourced warm and saline water masses into the subtropical intermediate North Atlantic can modify its deep thermocline at ~500–800 m (Fig. 2)²². Increased MOW presence thereby weakens the stratification at mid-depth in the North Atlantic (Fig. 2) and increases the heat advection along isopycnals from the mid-latitude subsurface to the surface of the subpolar North Atlantic²³. The formation of this subsurface channel allows heat accumulated at mid-depth of the equatorial and subtropical Atlantic to be transported northwards independent of temperature changes at surface-water level²³. Hence, increased MOW production and its potential to channel heat at subsurface levels towards the North could explain the anomalous surface warming in the high-latitude North Atlantic during the Plio–Pleistocene transition. Notably, this potential synergetic link between MOW and high-latitude SST variability in the North Atlantic has thus far not been considered in numerical models because they lack the proper representation of the outflow due to the narrow width and shallow depth of the Strait of Gibraltar.

Here we investigate the relationship between MOW production and high-latitude North Atlantic SST variability during the iNHG. We integrate numerical modelling with proxy data to approximate MOW strength and its impact on temperature in the North Atlantic and compare our results with existing SST records. The MOW strength reconstruction is based on X-ray fluorescence (XRF) scanning results from Site U1389²⁴ located in the Gulf of Cadiz and existing records of hydroclimate variability in the Mediterranean realm. The impact of MOW intrusion on the North Atlantic hydrography is estimated via the atmosphere–ocean–sea-ice–vegetation model COSMOS (Community Earth System Models) under Pliocene boundary conditions.

Results and discussion

MOW variability during the Plio–Pleistocene transition. To reconstruct MOW strength, we approximate its flow speed that is proportional to its volume flux²⁵ by using the sedimentary ln(Zr/Al) ratio determined by XRF core scanning (see “Methods”)^{26,27}. This proxy follows the rationale that high bottom flow speeds favour the accumulation of heavy minerals relative to the less dense aluminosilicates²⁶. Hence, a high ln(Zr/Al) ratio reflecting a high MOW flow speed also indicates an increased volume flux as well as strength, and vice versa. The temporal ln(Zr/Al) evolution at Site U1389 clearly depicts cyclical changes of the MOW production between 3.1 and 2.55 Ma (see Fig. 3). In fact, the spectral analyses of the ln(Zr/Al) record reveal a persistent precession pacing with a spectral peak at ~20 kyr (Fig. S2; Supplementary Methods). The distinct modulations of MOW strength by precession derive from the well-documented intimate link between MOW and monsoon controlled freshwater discharge into its eastern Mediterranean source region^{28–30}. There, surface-water freshening disrupts intermediate convection—and thus the formation of MOW source waters—when monsoonal runoff

enters the eastern Mediterranean Sea via the River Nile^{28,30}. This situation occurs during precession minima. In contrast, during precession maxima (i.e. low NH summer insolation) the North East African monsoonal system is positioned further to the south, which reduces Nile River runoff and by extension fosters MOW formation^{31,32}.

The interval between ~2.9 and 2.7 Ma (Fig. 3b; glacials G14–G7) of Site U1389 is characterized by the repeated occurrence of sandy layers (see Fig. S3). The high sand contents of the drift deposits are particular susceptible of being washed out during the rotary drilling process³³ and prohibited continuous XRF-scanning (gaps in the ln(Zr/Al) record). The coarsening of the sediment between ~2.9 and 2.7 Ma implies an intensified MOW production that caused an exceptionally high flow speed regime along the continental slope of the Gulf of Cadiz. This led to increased winnowing and enhanced sand-sized particle deposition as observed at Site U1389^{25,26,28,30}. Widespread erosive features and enhanced sand contents testifying to enhanced MOW flow speed during this time interval are also found in seismic profiles and sediment cores across the Gulf of Cadiz^{33,34}. Thus, the improved core recovery of the time intervals preceding, and subsequent to, the intensified MOW interval (here termed “iMOW” interval), as evident from the recorded ln(Zr/Al) variability, points to overall reduced sand contents in these drift deposits, and in extension to reduced overall MOW production.

To support our inference of increased MOW production during the iMOW interval, we assessed the fresh water input to its Mediterranean source region by comparing our MOW flow reconstruction to the North African aridity index of ODP Site 967 (Fig. 3a, b) located in the Levantine Basin (Fig. 2)^{35,36}. We find that the proposed tight coupling between MOW production and North African hydroclimate is supported by the significant correlation between the ln(Zr/Al) record and the North African aridity index for our study interval (Fig. S4; Supplementary Methods). Interestingly, during the iMOW interval between ~2.9 and 2.7 Ma North Africa experienced a strong increase in aridity (Fig. 3a, b), which is potentially linked to the simultaneous ~2.4 Ma eccentricity minimum. In fact, results from numeric modelling as well as proxy data analyses have demonstrated a tight but non-linear linkage between the Mediterranean freshwater budget and changes in Earth’s orbital configuration^{31,37–39}. During a pronounced eccentricity minimum, the precession amplitude is strongly muted which, according to numerical model and proxy data, causes a substantial weakening of the African monsoonal system^{31,40}. This can lead to a reduction of continental runoff into the Mediterranean of up to -2×10^{15} lyr^{-1} and thus facilitate an increase of Mediterranean salinity by up to ~10 PSU³⁸. In fact, we find a maximum ~2.5% increase of benthic $\delta^{18}\text{O}_{\text{ivf-sw}}$, reflecting intermediate water depth salinities in the western Mediterranean basin, coinciding with the iMOW phase (Fig. 3d)⁴¹. This indicates that the salinity of the MOW was enhanced by up to ~7 PSU during the iMOW phase relative to the time intervals 3.1–2.9 and 2.7–2.6 Ma, respectively (see “Methods” for discussion about the conversion of $\delta^{18}\text{O}_{\text{ivf-sw}}$ into salinity)⁴¹. This supports our finding that during the iMOW phase strong North African aridity facilitated a substantial increase in Mediterranean water salinity and consequently enhanced MOW production as documented by the erosional features along the continual slope of the Gulf of Cadiz.

Influence of MOW on the North Atlantic heat distribution. To assess the potential effect of increased MOW intrusion on the spatial heat distribution of the mid-latitude North Atlantic, and its potential for explaining the anomalous high-latitude SST warming between 2.9 and 2.7 Ma, we simulated the injection

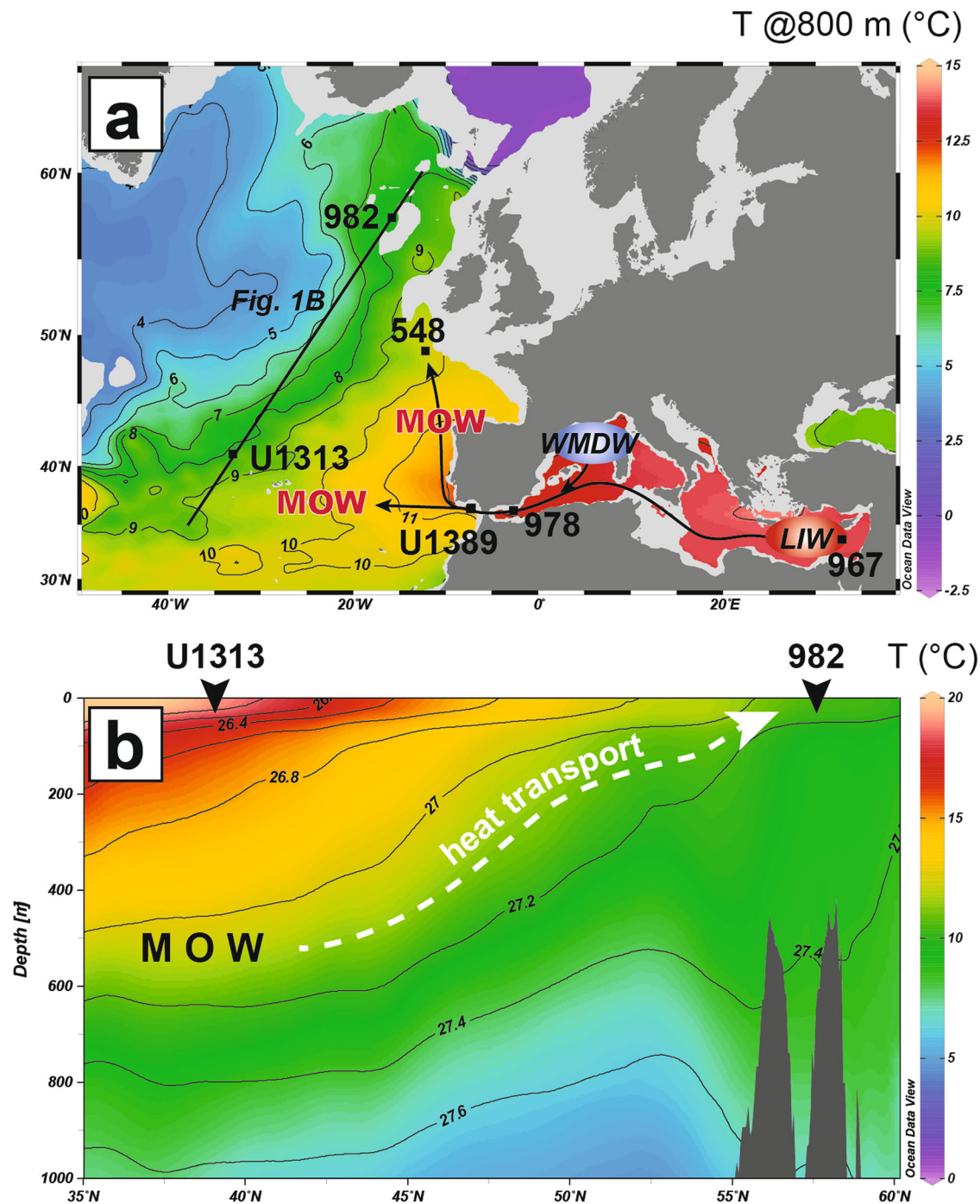


Fig. 2 Hydrography of the North Atlantic and Mediterranean Sea. **a** Temperatures at 800 m water depth in the North Atlantic. Denoted are sites referenced in the text as well as the major flow paths of the Levantine Intermediate Water (LIW), Western Mediterranean Deep Water (WMDW) and the Mediterranean Outflow Water (MOW)⁶⁵. Hydrographic section displayed in **(b)** is indicated by a black line. **b** Meridional hydrographic section through Sites U1313 and 982 with temperatures (shading) and isopycnals (kg m^{-3} ; contours). The MOW is indicated by a positive temperature anomaly in the deep thermocline at approximately 400–1000 m water depth, decreasing upper ocean stratification. The present-day northward trajectory of isopycnal heat transport is indicated by a white dashed arrow.

of MOW into the intermediate North Atlantic under Pliocene boundary conditions utilizing a modification of the PlioMIP2 setup of the COSMOS (see “Methods”). To image the heat transport across the entire North Atlantic basin, we analysed heat anomalies along a meridional (30°N – 55°N ; 20°W ; Fig. 4) and zonal (10°W – 45°W ; 40°N ; Fig. 4) cross-section of the North Atlantic, respectively. We find that the MOW intrusion has a two-fold effect on North Atlantic hydrography: firstly, the zonal

section (Fig. 4a) indicates that the MOW plume settles dominantly at intermediate water depth (800–000 m) during its westward propagation leading to a warming of $\sim 2^{\circ}\text{C}$ in the mid-Atlantic; secondly, the model results highlight the formation of a subsurface heat channel (Fig. 4b) that seemingly traverses the accumulated subtropical heat from intermediate water depths towards the surface of the high-latitude North Atlantic ($>50^{\circ}\text{N}$) where a surface warming of ~ 2 – 3°C can be observed—a process

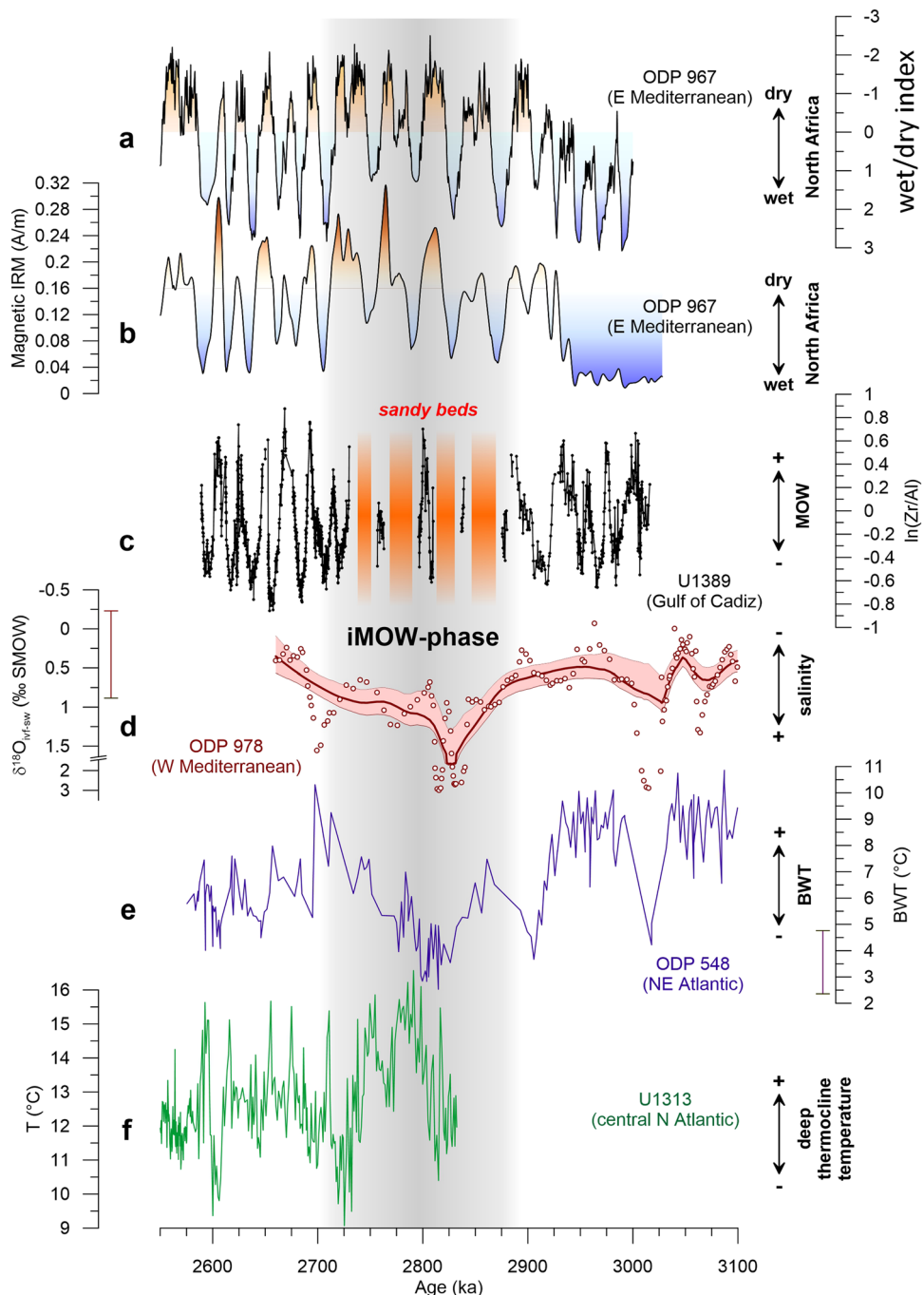


Fig. 3 The impact of Mediterranean Outflow Water (MOW) on the North Atlantic during the Plio-Pleistocene transition. **a** Wet-dry index from ODP Site 967 (see Fig. 2 for site location).³⁵ **b** Hematite record from ODP Site 967.³⁶ **c** $\ln(\text{Zr}/\text{Al})$ ratio as a measure for MOW production (this study); presumed sandy beds hampering core recovery are indicated by red bars. **d** Ice volume corrected $\delta^{18}\text{O}$ of the bottom water ($\delta^{18}\text{O}_{\text{ivf-sw}}$) as a measure of western Mediterranean deep-water salinity from Site 978 (red symbols; red line denotes LOESS smoothing by factor 0.07, shading indicates 95% confidence interval).⁴¹ **e** Mg/Ca-derived bottom water temperature (BWT) of DSDP Site 548 (blue line; see Fig. 2 for site location).⁴¹ **f** Thermocline temperature of Site U1313 based on *Globorotalia crassaformis*.⁶⁶ Grey shading indicates the interval of anomalous intensive MOW flow speed ("iMOW" phase) leading to the deposition of sandy contourites and poor core recovery in the Gulf of Cadiz at IODP Site 1389 (see Fig. 2 for site location).³³

that thus might very well explain the observed high-latitude warming during the iMOW interval of $\sim 2^\circ\text{C}$.

This subsurface heat transport strongly resembles results from modern drifter studies on the heat connectivity between subtropical and subpolar gyres. These results indicate that the communication between both gyres is at the surface level strongly limited due to a strong vorticity gradient^{23,42}. As the vorticity gradient between both gyre systems decreases with increasing

water depth the heat stored within the subtropical gyre can be channelled north along isopycnals that outcrop in the subpolar gyre.²³ The injection of heat by the MOW below the subtropical gyre deepens the subtropical thermocline and thickens the density layers through which subtropical waters reach the subpolar gyre. Thick isopycnals increase the subtropical–subpolar flow at levels not constrained by vorticity gradients (Fig. 2). Therefore, the MOW provides a channel for subtropical waters to reach higher

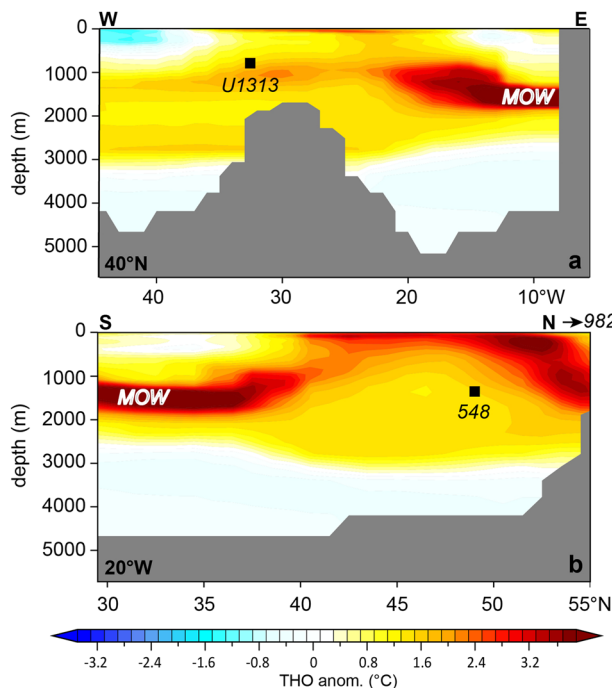


Fig. 4 Temperature anomaly (based on simulated potential seawater temperature, MPIOM variable THO) between the PlioMIP2 Pliocene background state of COSMOS and the simulation with added Newtonian salinity restoring mimicking the Mediterranean Overflow Water (MOW).

a Intrusion along a meridional transect (30° – 55° N; 20° W) and (b) zonal cross-section (10° – 45° W; 40° N) of the North Atlantic. Locations of referenced data sets from Sites U1313 and DSDP548 are indicated.

latitudes and its effect can be assessed by the thermal gradient between the surface and deep thermocline at mid-latitudes. Modern hydrographic data show that the injection of dense MOW decreases the stratification of the mid-latitude North Atlantic and thus opens this subsurface heat channel, which supplies warmth to high latitudes (Fig. 2).

If this hypothesized subsurface heat channel was particularly active during the iMOW interval, as the model results suggest, it should have left traces in available temperature reconstructions from the intermediate subtropical (IODP Site U1313; $41^{\circ}0'0''$ N, $32^{\circ}57'26.3''$ W, 3200 m)⁴³ and mid-latitude (DSDP Site 548; $48^{\circ}54'56.8''$ N, $12^{\circ}9'50.4''$ W; 1200 m)⁴¹ North Atlantic (Fig. 2). Indeed, within the iMOW interval, at ~ 2.8 Ma we find a warming of ~ 3 °C of intermediate water depths (~ 800 m) of the central North Atlantic IODP Site U1313 (Fig. 3f)⁴³. This temperature increase argues for a heat accumulation at subsurface levels and thus strongly mimics the model predictions for the zonal MOW behaviour, also in terms of magnitude. In contrast, we observe a cooling of ~ 4 °C of intermediate waters (~ 1200 m water depth) at Site DSDP Site 548 during the iMOW interval, reaching lowest temperatures at ~ 2.8 Ma (Figs. 2 and 3e). Under modern conditions, Site DSDP 548 is bathed in the northward propagating branch of the MOW⁴¹. Thus, the temperature decline argues for the absence or substantially reduced influence of MOW at this site during the iMOW interval. Based on our model results, this lack of MOW influence at Site DSDP Site 548 during the iMOW interval originates from a shoaling of the MOW plume, which is also in line with previous suggestions⁴¹. Hence, the modelled heat anomalies across the intermediate-depth North Atlantic generated by strong MOW production are in good agreement with proxy evidence. This is particularly noticeable when considering the limitations of the model to resolve spatially complex

hydrographic conditions such as prevalent along the European margin, which is related to limited spatial resolution towards enabling long-term integrations for paleoclimatic applications. The ability to represent the impact of MOW on the oceanic heat distribution in a low-resolution model setup hints that the subsurface heat channel across the Atlantic Ocean may be a robust feature of past, present and future ocean circulation.

A long-term perspective of MOW influence on the North Atlantic. To assess the potential of this subsurface heat channel during other time periods, we analysed the existing mid- to high-latitude SST records back to 3.6 Ma when MOW started to intrude into the North Atlantic on a similar scale as today^{34,41}. In fact, we find that when considering long-term trends, a similar anomalous high-latitude warming phase in the North Atlantic between 3.5 and 3.1 Ma dovetails strongly increased salinities in the western Mediterranean Sea (Fig. 5) as well as coincides with similar timed erosional features along the continental slope of the Gulf of Cadiz³⁴. This provides strong indications that an enhanced MOW production and development of a subsurface heat channel between the mid and high latitudes in the North Atlantic might have been active during the glacial period M2 (~ 3.3 Ma) as well as during the high $p\text{CO}_2$ period KM5c (3.21–3.19 Ma)⁴⁴. However, a detailed study of this interval, in contrast to the 2.9–2.7 Ma interval, is currently not possible due to poor preservation of the sedimentary sequence from the Gulf of Cadiz prior to ~ 3.2 Ma as well as the lack of intermediate-water-mass records from the mid-latitude North Atlantic.

An active subsurface heat channel driven by strong MOW production during KM5c, considered an analogue for future climate change⁴⁵, might nevertheless provide a blueprint of its impact on the North Atlantic hydrography under increasing $p\text{CO}_2$ levels. Model results show that during KM5c the Mediterranean experienced 2–3 °C warmer temperatures, shifting its hydrological balance into greater net loss of freshwater⁴⁶. This is a similar climate development as predicted for the Mediterranean region until the year 2100^{47,48}. Consequently, the lack of freshwater influx to the Mediterranean during KM5c probably boosted its salinities and with it MOW production (Fig. 5). The increased MOW production then might also have led to a rerouting of heat to the high-latitude North Atlantic via the subsurface aligning with established SST dynamics for this time period⁸. Our mechanism thus provides an explanation for the observed high-latitude SST anomaly during KM5c, which has been commonly attributed to polar amplification instead⁴⁵.

In summary, we argue that a MOW-driven subsurface heat channel might have played a role in delaying Northern Hemisphere ice sheet growth against the backdrop of global cooling and declining $p\text{CO}_2$ whilst also holding insights into the SST evolution of the North Atlantic under future climate scenarios. As aridity is projected to increase severely in the circum-Mediterranean region until the year 2100⁴⁷, we expect MOW production to increase in the future. This in turn would invigorate the subsurface heat transport to the high-latitude North Atlantic, as indicated for the interval of KM5c, and thus potentially further amplify the effects of global warming in this climatically extremely sensitive region.

Methods

Reconstructing MOW flux variability at IODP Site U1389. For the reconstruction of MOW flow strength variability during the Plio-Pleistocene transition (3.1–2.6 Ma), we utilized sediment cores from IODP Site U1389 ($36^{\circ}25'N$, $7^{\circ}16'W$; 644 m water depth) located in proximity to the Gibraltar Strait, and thus directly influenced by the MOW²⁸. The Late Pliocene age model of Site U1389 is well constrained by correlation of the planktonic $\delta^{18}\text{O}$ records of ODP Site 978 in the Alboran Sea⁴¹ and the Rossello section on Sicily (see²⁷ for details on the Pliocene stratigraphy of Site U1389). Split cores were analysed with an Avaatech X-ray

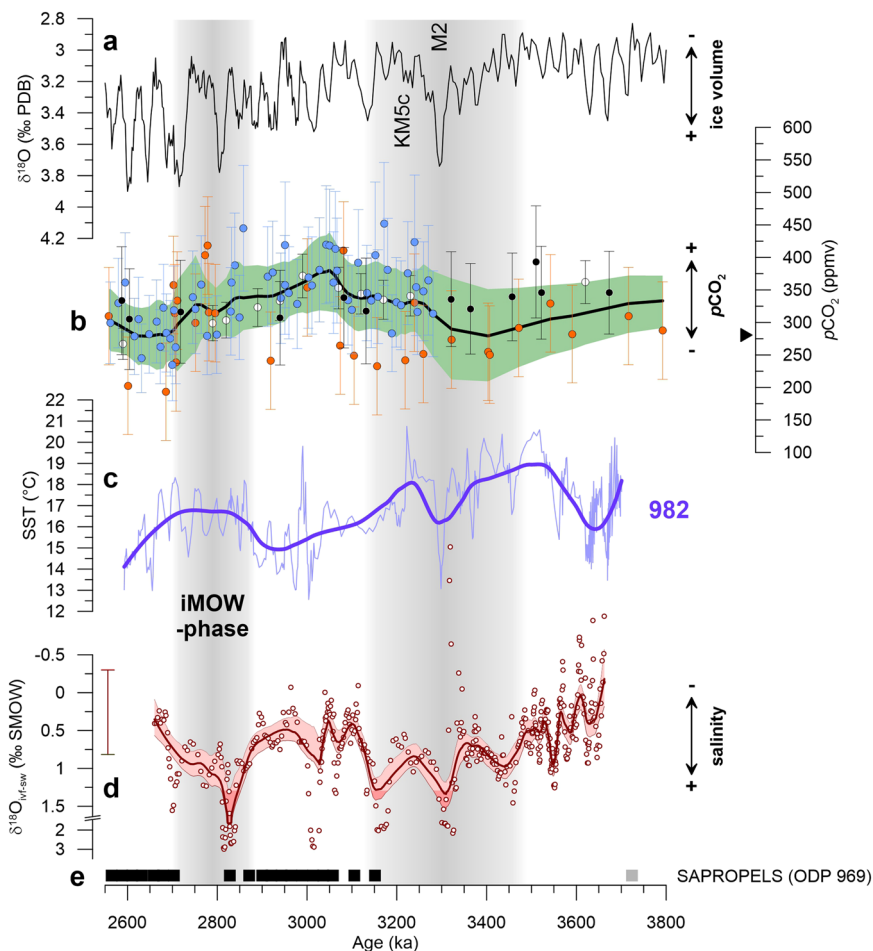


Fig. 5 Relation of North Atlantic sea surface warming and MOW activity from 3.8–2.6 Ma. **a** Ice volume reconstruction with Glacial M2 and warmphase KM5c denoted⁴⁴. **(b)** different atmospheric $p\text{CO}_2$ reconstructions for the Plio-Pleistocene transition (white circles²; orange circles³; blue circles⁴); with LOESS smoother (black line; factor: 0.07) and 95% confidence interval (green shading) derived from a Monte Carlo Simulation with 1000 iterations. **c** Sea surface temperatures (SST) of high-latitude site ODP Site 982⁶⁴ on the revised age model of⁴¹, the data have been LOESS-smoothed (factor: 0.2). **d** Ice volume corrected $\delta^{18}\text{O}$ of the bottom water ($\delta^{18}\text{O}_{\text{ivf-sw}}$) as a measure of western Mediterranean deep-water salinity from Site 978 (red symbols; red line denotes LOESS smoothing by factor 0.07, shading indicates 95% confidence interval)⁴¹. **e** Sapropels (representing wet phases) in Eastern Mediterranean Site 969⁶⁷. The grey shadings indicate intervals of anomalous SST warming in the high-latitude North Atlantic concomitant to inferred increases in MOW production, including the “iMOW-Phase” discussed in the text.

Fluorescence (XRF) Core Scanner at the Center for Marine Environmental Sciences (MARUM, University of Bremen). Measurements were carried out at a resolution of 5 cm, integrated over a 1.2 cm^2 area with a 10 mm down-core slit size, with separate runs performed using generator settings of 10, 30 and 50 kV and currents of 0.2 and 1.0 mA, respectively. Sampling time was set to 20 s.

Reconstructing $\delta^{18}\text{O}_{\text{ivf-sw}}$ from ODP Site 978 (Alboran Sea). Increased MOW production is tightly linked to increased salinities of the intermediate- and deep-water masses of the Mediterranean Sea^{20,49}. In fact, Levantine Intermediate Water (LIW) and the upper portion of the Western Mediterranean Deep Water (uWMDW) are the main contributors to the MOW^{20,49}. The LIW is formed in the eastern Mediterranean Sea in the highly evaporative Levantine Basin during wintertime cooling. It feeds into the uWMDW that originates in the Gulf of Lyons and constitutes the densest portion of the MOW²⁰. During strong North African aridity phases, the fresh water supply to the Mediterranean, e.g. by strong Nile discharge, is suppressed, increasing the salinity of the Mediterranean intermediate- and deep-water masses and in turn enhancing MOW formation^{28,30,31}.

To reconstruct the salinity of the uWMDW as a measure of MOW production, we utilized the existing stable oxygen isotope ($\delta^{18}\text{O}$) and Mg/Ca-based bottom water temperatures (BWT) derived from benthic foraminifera *Cibicides* spp. from Site ODP 978 in the Alboran Sea⁴¹. Site ODP 978 is located in the Alboran Sea north of the Al-Mansour Seamount ($36^{\circ}13'\text{N}$, $02^{\circ}03'\text{W}$; Fig. 2) at ~ 1920 m water depth, and is thus bathed in uWMDW⁴¹. The preliminary age model of Site ODP 978 was slightly adapted in this study by visually matching the benthic $\delta^{18}\text{O}$ from Site ODP 978 to the LR04 stack⁴⁴. For paleo-salinity reconstructions, we calculated the $\delta^{18}\text{O}$ of sea water ($\delta^{18}\text{O}_{\text{sw}}$) by applying the *Cibicides* spp.-specific equation of⁵⁰ to the measured $\delta^{18}\text{O}$ using the Mg/Ca-based BWT provided by⁴¹. The resultant

$\delta^{18}\text{O}_{\text{sw}}$ were corrected for the ice-volume effects ($\delta^{18}\text{O}_{\text{sw-ivf}}$) following⁵¹ by using the eustatic sea level reconstruction of⁵².

Modelling the influence of MOW on the North Atlantic water column. The COSMOS PlioMIP2 core simulation Eoi400⁴⁸ was chosen as a starting point for studying the impact of MOW on the North Atlantic hydrography during the Plio-Pleistocene transition⁴⁸. It is based on the state-of-the-art reconstruction of mid-Piacenzian paleoenvironment by⁵³. Consequently, it provides a reference setup that considers best knowledge on the mid-Pliocene state of ice sheets, configuration of continents and ocean gateways, as well as carbon dioxide concentrations. However, the COSMOS PlioMIP2 core simulation does not include MOW injection into the North Atlantic and, furthermore, the topographic details of the Strait of Gibraltar are limited due to the coarse spatial resolution of the ocean model ($\sim 3.0^\circ \times 1.9^\circ$ formally at a bipolar curvilinear model grid). Hence, to simulate the intrusion of MOW and to analyse its impact on North Atlantic circulation and hydrography, we implemented a prolonged Newtonian salinity restoring towards a reference salinity of 45 PSU at the Strait of Gibraltar (34°N , 352°E) at intermediate water depth (about 700 m). The 45 PSU input MOW salinity is derived from converting the maximum $\delta^{18}\text{O}_{\text{sw-ivf}}$ from ODP Site 978 (Alboran Sea) into bottom-water salinity (PSU) by applying the modern Mediterranean Sea-specific $\delta^{18}\text{O}_{\text{sw-ivf}}$ -salinity relationship following⁵⁴. We argue that because Late Pliocene background conditions are comparable to modern in terms of paleogeography and climate^{41,55}, the applied modern Mediterranean Sea $\delta^{18}\text{O}_{\text{sw-ivf}}$ -salinity relationship can be used as an approximation. This assumption is supported by numerical model simulations for the Late Pliocene that suggest a similar $\delta^{18}\text{O}_{\text{sw-ivf}}$ -salinity relationship between Modern and Late Pliocene, and even highlight an increase in Mediterranean surface salinity under Late Pliocene

boundary conditions as proposed in this study⁵⁵. Notably, the modelled global ocean $\delta^{18}\text{O}_{\text{sw-ivf}}$ –salinity relationship for the Late Pliocene has an even smaller slope (0.22)⁵⁵ than the modern one (0.27)⁵⁴, which would generate even higher salinities for the MOW in comparison to our conservative estimates based on the modern $\delta^{18}\text{O}_{\text{sw-ivf}}$ –salinity relationship⁵⁴.

Based on our model simulations, the denser MOW flow core during the iMOW interval settles at roughly ~1200 m water depth within the North Atlantic (Fig. 4), which is deeper than its modern main flow core depth between 500 and 800 m water along the continental slope of the Gulf of Cadiz^{28,30}. Notably, the simulated model depth is in line with MOW flow core settling depth reconstructions from the Last Glacial Maximum when a MOW with higher-than-modern salinity (<40 PSU) settled at water depths of roughly 800–1200 m⁵⁶. Hence, the simulated heat transport already does take into account the deeper MOW flow path as a consequence of the increased salinity.

Starting point of this modelling study is a quasi-equilibrium mid-Pliocene climate state derived from the COSMOS PlioMIP2 mid-Pliocene core simulation Eo1400⁴⁸. We initialized the model from the mid-Pliocene core climate state after a model spin-up over 1400 model years. The climate simulation was integrated thereafter with Newtonian salinity restoring as described above. The strength of the AMOC reacted to the implied more saline MOW with an overshoot after about 1750 model years. The impact of the mimicked MOW salinification on the hydrography of the North Atlantic Ocean is investigated based on this AMOC overshoot.

COSMOS model description. The Community Earth System Models (COSMOS) provide a numerical representation of the coupled atmosphere–ocean–land system with explicit consideration of the land-surface carbon cycle, including dynamic vegetation. The climate system is represented by the atmospheric general circulation model ECHAM5⁵⁷ with river runoff scheme, the land surface and carbon cycle model JSBACH⁵⁸ with vegetation dynamics⁵⁹, and the ocean general circulation model MPIOM⁶⁰ with a dynamic-thermodynamic sea ice scheme based on the model by⁶¹. The COSMOS has been applied with a resolution of T31 ($3.75^\circ \times 3.75^\circ$) and 19 hybrid sigma-pressure levels in the atmosphere and a bipolar curvilinear GR30 grid with formal resolution of $\sim 1.8^\circ \times 3.0^\circ$ and 40 z-levels in the ocean domain. Ocean and atmosphere are coupled once per model day via the OASIS3 coupler⁶². Time steps of atmosphere and ocean are 2400 and 8640 s, respectively. Methods employed in COSMOS towards improvement of ocean circulation at coarse model resolution are outlined in the literature; for an overview see⁶³ as well as⁴⁸, who present a detailed description of the model and of its application in the framework of paleoclimate research. The model does not necessitate any flux corrections. Beyond the implementation of Newtonian salinity restoring at the Strait of Gibraltar towards mimicking more saline MOW, we have not applied any artificial fluxes in the model setup.

Simulating the impact of MOW in the COSMOS model. Towards mimicking more saline MOW in the model, we perform a localized restoring of salinity (S) towards a target value S_{ref} that is chosen to represent the characteristics of MOW (see above). The parameterization of high-saline Mediterranean Outflow via Newtonian salinity restoring is performed at one grid cell at a depth of about 700 m at the Strait of Gibraltar (34°N , 352°E) following Eq. 1.

$$S_{\text{new}} = S_{\text{old}} + f \cdot (S_{\text{ref}} - S_{\text{old}}) \quad (1)$$

The ocean model locally restores salinity towards the, in comparison to the simulated salinity, increased target value ($S_{\text{ref}} = 45.0$) by computing a new salinity (S_{new}) that is based on the salinity S_{old} of the previous time step and a restoring time-constant (f) of $10.368 \times 10^6 \text{ s}^{-1}$ that refers to a time period of 4 months.

Overshoots in the AMOC, which result from the application of Newtonian salinity restoring, represent a surrogate to the impact of more saline MOW on large-scale circulation and oceanographic patterns of the Pliocene Atlantic Ocean.

Data availability

All referenced data sets are online available via pangea.de. The model data of the COSMOS PlioMIP2 mid-Pliocene core simulation and the respective pre-industrial control state are available from a repository at the University of Leeds (<ftp://see-gw-01.leeds.ac.uk>).

Received: 17 January 2021; Accepted: 12 July 2021;

Published online: 10 August 2021

References

- Mudelsee, M. & Raymo, M. E. Slow dynamics of the Northern Hemisphere glaciation. *Paleoceanography* **20**, PA4022 (2005).
- Seki, O. et al. Alkenone and boron-based Pliocene $p\text{CO}_2$ records. *Earth Planet. Sci. Lett.* **292**, 201–211 (2010).
- Bartoli, G., Sarnthein, M. & Weinelt, M. Late Pliocene millennial-scale climate variability in the northern North Atlantic prior to and after the onset of Northern Hemisphere glaciation. *Paleoceanography* **21**, PA4205 (2006).
- Martinez-Botí, M. A. et al. Boron isotope evidence for oceanic carbon dioxide leakage during the last deglaciation. *Nature* **518**, 219–222 (2015).
- Haug, G. H. & Tiedemann, R. Effect of the formation of the isthmus of panama on Atlantic Ocean thermohaline circulation. *Nature* **393**, 673–676 (1998).
- Karas, C. et al. Mid-Pliocene climate change amplified by a switch in Indonesian subsurface throughflow. *Nat. Geosci.* **2**, 434–438 (2009).
- Karas, C. et al. Pliocene oceanic seaways and global climate. *Sci. Rep.* **7**, 1–8 (2017).
- Naafs, B. D. A. et al. Repeated near-collapse of the Pliocene sea surface temperature gradient in the North Atlantic. *Paleoceanogr. Paleoclimatol.* **35**, e2020PA003905 (2020).
- Klocker, A., Prange, M. & Schulz, M. Testing the influence of the Central American Seaway on orbitally forced Northern Hemisphere glaciation. *Geophys. Res. Lett.* **32**, L03703 (2005).
- Haug, G. H. et al. North Pacific seasonality and the glaciation of North America 2.7 million years ago. *Nature* **433**, 821–825 (2005).
- DeConto, R. M. et al. Thresholds for Cenozoic bipolar glaciation. *Nature* **455**, 652–656 (2008).
- Rahmstorf, S. Ocean circulation and climate during the past 120,000 years. *Nature* **419**, 207–214 (2002).
- Caesar, L. et al. Observed fingerprint of a weakening Atlantic Ocean overturning circulation. *Nature* **556**, 191–196 (2018).
- Naafs, B. D. A. et al. Late Pliocene changes in the North Atlantic Current. *Earth Planet. Sci. Lett.* **298**, 434–442 (2010).
- Otto-Btiesner, B. L. et al. Amplified North Atlantic warming in the Late Pliocene by changes in Arctic gateways. *Geophys. Res. Lett.* **44**, 957–964 (2017).
- Auderset, A. et al. Gulf Stream intensification after the Early Pliocene shoaling of the Central American Seaway. *Earth Planet. Sci. Lett.* **520**, 268–278 (2019).
- Matthiessen, J. et al. Pliocene palaeoceanography of the Arctic Ocean and subarctic seas. *Philos. Trans. R. Soc. A* **367**, 21–48 (2009).
- Schneider, B. & Schmittner, A. Simulating the impact of the Panamanian seaway closure on ocean circulation, marine productivity and nutrient cycling. *Earth Planet. Sci. Lett.* **246**, 367–380 (2006).
- Zhang, X. et al. Changes in equatorial Pacific thermocline depth in response to Panamanian seaway closure: insights from a multi-model study. *Earth Planet. Sci. Lett.* **317**, 76–84 (2012).
- Millot, C. Heterogeneities of in- and out-flows in the Mediterranean Sea. *Prog. Oceanogr.* **120**, 254–278 (2014).
- Rogerson, M. et al. Paleoceanography of the Atlantic-Mediterranean exchange: overview and first quantitative assessment of climatic forcing. *Rev. Geophys.* **50**, RG2003 (2012).
- Potter, R. A. & Lozier, M. S. On the warming and salinification of the Mediterranean Outflow Waters in the North Atlantic. *Geophys. Res. Lett.* **31**, L01202 (2004).
- Foukal, N. P. & Lozier, M. S. No inter-gyre pathway for sea-surface temperature anomalies in the North Atlantic. *Nat. Commun.* **7**, 11333 (2016).
- Sarnthein, M. et al. Interhemispheric teleconnections: Late Pliocene change in Mediterranean Outflow Water linked to changes in Indonesian through-flow and Atlantic Meridional Overturning Circulation, a review and update. *Int. J. Earth Sci.* **107**, 505–525 (2018).
- Kaboth-Bahr, S. et al. Monsoonal forcing of European ice-sheet dynamics during the Late Quaternary. *Geophys. Res. Lett.* **45**, 7066–7074 (2018).
- Bahr, A. et al. Deciphering bottom current velocity and paleoclimate signals from contourite deposits in the Gulf of Cadiz during the last 140 kyr: an inorganic geochemical approach. *Geochem. Geophys. Geosystems* **15**, 3145–3160 (2014).
- Grunert, P. et al. Revised and refined age model for the upper Pliocene of IODP Site U1389 (IODP Expedition 339, Gulf of Cádiz). *Newsletters Stratigr.* **51**, 261–283 (2017).
- Bahr, A. et al. Persistent monsoonal forcing of Mediterranean Outflow Water dynamics during the Late Pleistocene. *Geology* **43**, 951–954 (2015).
- Kaboth, S. et al. Mediterranean Outflow Water dynamics during the past ~570 kyr: regional and global implications. *Paleoceanography* **32**, 634–647 (2017).
- Kaboth, S. et al. New insights into upper MOW variability over the last 150 kyr from IODP 339 Site U1386 in the Gulf of Cadiz. *Mar. Geol.* **377**, 136–145 (2016).
- Rohling, E. J., Marino, G. & Grant, K. M. Mediterranean climate and oceanography, and the periodic development of anoxic events (sapropels). *Earth-Sci. Rev.* **143**, 62–97 (2015).
- Rossignol-Strick, M. African monsoons, an immediate climate response to orbital insolation. *Nature* **304**, 46–49 (1983).
- Stow, D. A. V., Hernández-Molina, F. J. & Alvarez-Zarikian, C. Expedition 339 summary. *Proc. IODP Expedition Vol. 339* (IODP, 2013).

34. Hernandez-Molina, F. J. et al. Onset of Mediterranean Outflow into the North Atlantic. *Science* **344**, 1244–1250 (2014).
35. Grant, K. M. et al. A 3 million year index for North African humidity/aridity and the implication of potential pan-African Humid Periods. *Quat. Sci. Rev.* **171**, 100–118 (2017).
36. Larrasoana, J. C. et al. Three million years of monsoon variability over the northern Sahara. *Clim. Dyn.* **21**, 689–698 (2003).
37. Rohling, E. J. et al. African monsoon variability during the previous interglacial maximum. *Earth Planet. Sci. Lett.* **202**, 61–75 (2002).
38. Simon, D. et al. Quantifying the Mediterranean freshwater budget throughout the Late Miocene: new implications for sapropel formation and the Messinian Salinity Crisis. *Earth Planet. Sci. Lett.* **472**, 25–37 (2017).
39. Bosmans, J. H. C. et al. Precession and obliquity forcing of the freshwater budget over the Mediterranean. *Quat. Sci. Rev.* **123**, 16–30 (2015).
40. Bosmans, J. H. C. et al. Response of the North African summer monsoon to precession and obliquity forcings in the EC-Earth GCM. *Clim. Dyn.* **44**, 279–297 (2014).
41. Khélifi, N. et al. Late Pliocene variations of the Mediterranean Outflow. *Mar. Geol.* **357**, 182–194 (2014).
42. Burkholder, K. C. & Lozier, M. S. Tracing the pathways of the upper limb of the North Atlantic Meridional Overturning Circulation. *Geophys. Res. Lett.* **41**, 4254–4260 (2014).
43. Naafs, B. D. A. et al. Strengthening of North American dust sources during the Late Pliocene (2.7 Ma). *Earth Planet. Sci. Lett.* **317**, 8–19 (2012).
44. Lisiecki, L. E. & Raymo, M. E. A Pliocene-Pleistocene stack of 57 globally distributed benthic $\delta^{18}\text{O}$ records. *Paleoceanography* **20**, 1–17 (2005).
45. McClymont, E. L. et al. Lessons from a high- CO_2 world: an ocean view from \sim 3 million years ago. *Clim. Past* **16**, 1599–1615 (2020).
46. Tan, N. et al. Modeling a modern-like $p\text{CO}_2$ warm period (Marine Isotope Stage KM5c) with two versions of an Institut Pierre Simon Laplace atmosphere-ocean coupled general circulation model. *Clim. Past* **16**, 1–16 (2020).
47. Gao, X. & Giorgi, F. Increased aridity in the Mediterranean region under greenhouse gas forcing estimated from high resolution simulations with a regional climate model. *Glob. Planet. Change* **62**, 195–209 (2008).
48. Stepanek, C., Samakinwa, E., Knorr, G. & Lohmann, G. Contribution of the coupled atmosphere-ocean-sea ice-vegetation model COSMOS to the PlioMIP2. *Clim. Past* **16**, 2275–2323 (2020).
49. Millot, C. et al. Large warming and salinification of the Mediterranean Outflow due to changes in its composition. *Deep Sea Res. I* **53**, 656–666 (2006).
50. Marchitto, T. M. et al. Improved oxygen isotope temperature calibrations for cosmopolitan benthic foraminifera. *Geochim. Cosmochim. Acta* **130**, 1–11 (2014).
51. Rohling, E. J. et al. Sea-level and deep-sea-temperature variability over the past 5.3 million years. *Nature* **508**, 477–482 (2014).
52. de Boer, B., Lourens, L. J. & van de Wal, R. S. W. Persistent 400,000-year variability of Antarctic ice volume and the carbon cycle is revealed throughout the Plio-Pleistocene. *Nat. Commun.* **5**, 2999 (2014).
53. Dowsett, H. et al. The PRISM4 (mid-Piacenzian) paleoenvironmental reconstruction. *Clim. Past* **12**, 1519–1538 (2016).
54. Pierre, C. The oxygen and carbon isotope distribution in the Mediterranean water masses. *Mar. Geol.* **153**, 41–55 (1999).
55. Tindall, J. C. & Haywood, A. M. Modeling oxygen isotopes in the Pliocene: large-scale features over the land and ocean. *Paleoceanography* **30**, 1183–1201 (2015).
56. van Dijk, J. et al. A saltier Glacial Mediterranean Outflow. *Paleoceanogr. Paleoclimatol.* **33**, 179–197 (2018).
57. Roeckner, E. et al. *The Atmospheric General Circulation Model ECHAM5: Part 1: Model Description*. MPI Report No. 34 (Max-Planck Institut für Meteorologie, Hamburg, 2003).
58. Raddatz, T. J. et al. Will the tropical land biosphere dominate the climate-carbon cycle feedback during the twenty-first century? *Clim. Dyn.* **29**, 565–574 (2007).
59. Brovkin, V. et al. Global biogeophysical interactions between forest and climate. *Geophys. Res. Lett.* **36**, L07405 (2009).
60. Marsland, S. J. et al. The Max-Planck-Institute global ocean/sea ice model with orthogonal curvilinear coordinates. *Ocean Model.* **5**, 91–127 (2003).
61. Hibler, D. A. Dynamic thermodynamic Sea Ice Model. *J. Phys. Oceanogr.* **9**, 815–846 (1979).
62. Valcke, S. et al. *OASIS3 Ocean Atmosphere Sea Ice Soil Users's Guide*. Technical Report TR/CMGC/03/69 (CERFACS Toulouse, 2003).
63. Stepanek, C. & Lohmann, G. Modelling mid-Pliocene climate with COSMOS. *Geosci. Model Dev.* **5**, 1221–1243 (2012).
64. Lawrence, K. T., Bailey, I. & Raymo, M. E. Re-evaluation of the age model for North Atlantic Ocean Site 982 – arguments for a return to the original chronology. *Clim. Past* **9**, 1–7 (2013).
65. Boyer, T. P. et al. *World Ocean Database 2013*. NOAA Atlas NESDIS 73 (NOAA, 2013).
66. Bolton, C. T. et al. North Atlantic midlatitude surface-circulation changes through the Plio-Pleistocene intensification of Northern Hemisphere Glaciation. *Paleoceanogr. Paleoclimatol.* **33**, 1186–1205 (2018).
67. Emeis, K.-C. et al. The sapropel record of the eastern Mediterranean Sea – results of Ocean Drilling Program Leg 160. *Paleogeogr. Paleoclimatol. Palaeoecol.* **158**, 371–395 (2000).

Acknowledgements

We would like to thank two anonymous reviewers for their careful handling of our manuscript and constructive comments. S.K.B. received funding from an Open-Topic Post-Doc fellowship of the University of Potsdam. C.S. acknowledges funding by the Helmholtz Climate Initiative REKLIM and the Alfred Wegener Institute (AWI) research programme PACES2. P.G. and A.G.G. received funding from Austrian Science Fund (FWF; project P25831-N29) and ECORD (ECORD Research Grant to A.G.G.). M.C.A.C. and A.B. received funding from the Deutsche Forschungsgemeinschaft (DFG) project BA 3809/8. C.S. acknowledges helpful discussions with Gerrit Lohmann, section head of Paleoclimate Dynamics at the AWI, on the implementation of Newtonian restoring in ocean models. C.K. received funding from ANID/Millennium Science Initiative/Millennium Nucleus Paleoclimate NCN17_079 and from DICYT project number 405.

Author contributions

S.K.B., A.B., M.C.A.C., C.K., M.Z., P.G. and C.S. designed the study. A.G.G. conducted XRF core scanning and data analysis. A.B. produced the figures. C.S. set up the modified Pliocene setup with Newtonian salinity restoring and performed the COSMOS simulations. All authors contributed to discussion and manuscript preparation.

Funding

Open Access funding enabled and organized by Projekt DEAL.

Competing interests

The authors declare no competing interests.

Additional information

Supplementary information The online version contains supplementary material available at <https://doi.org/10.1038/s43247-021-00232-5>.

Correspondence and requests for materials should be addressed to S.K.B.

Peer review information *Communications Earth & Environment* thanks the anonymous reviewers for their contribution to the peer review of this work. Primary Handling Editors: Rachael Rhodes, Joe Aslin, Heike Langenberg. Peer reviewer reports are available.

Reprints and permission information is available at <http://www.nature.com/reprints>

Publisher's note Springer Nature remains neutral with regard to jurisdictional claims in published maps and institutional affiliations.



Open Access This article is licensed under a Creative Commons Attribution 4.0 International License, which permits use, sharing, adaptation, distribution and reproduction in any medium or format, as long as you give appropriate credit to the original author(s) and the source, provide a link to the Creative Commons license, and indicate if changes were made. The images or other third party material in this article are included in the article's Creative Commons license, unless indicated otherwise in a credit line to the material. If material is not included in the article's Creative Commons license and your intended use is not permitted by statutory regulation or exceeds the permitted use, you will need to obtain permission directly from the copyright holder. To view a copy of this license, visit <http://creativecommons.org/licenses/by/4.0/>.

© The Author(s) 2021